J. Fluid Mech. (2020), *vol.* 889, A8. © The Author(s), 2020.
Published by Cambridge University Press
doi:10.1017/jfm.2020.77

A momentum-conserving wake superposition method for wind farm power prediction

Haohua Zong[1,†] **and Fernando Porté-Agel**[1]

[1]Wind Engineering and Renewable Energy Laboratory (WIRE), École Polytechnique Fédérale de Lausanne (EPFL), EPFL-ENAC-IIE-WIRE, 1015 Lausanne, Switzerland

(Received 1 October 2019; revised 10 January 2020; accepted 22 January 2020)

Analytical wind turbine wake models and wake superposition methods are prevailing tools widely adopted by the wind energy community to predict the power production of wind farms. However, none of the existing wake superposition methods conserve the streamwise momentum. In this study, a novel wake superposition method capable of conserving the total momentum deficit in the streamwise direction is derived theoretically, and its performance is validated with both particle imaging velocimetry measurements and large-eddy simulation results. Detailed inter-method comparisons show that the novel wake superposition method outperforms all the existing methods by delivering an accurate prediction of the power production and the centreline wake velocity deficit, with a typical error of less than 5 % (excluding the near-wake region). Additionally, the momentum-conserving wake superposition method is extended to combine the transverse velocities induced by yawed wind turbines, and the secondary wake steering effect crucial to the power optimization in active wake control is well reproduced.

Key words: wakes

1. Introduction

Large wind farms with dozens of wind turbines arranged in multiple rows are increasingly built worldwide to reduce the usage of unsustainable fossil fuels. The spacing between the adjacent turbine rows/columns is typically selected as 3–10 times the rotor diameter, due to the limitations of land usage and connection cable length. At such a spacing, the power losses caused by the inevitable wake interactions can reach up to approximately 40 %, when the directions of turbine rows/columns are aligned with the wind direction (Stevens & Meneveau 2017; Porté-Agel, Bastankhah & Shamsoddin 2019). To minimize these power losses, a fast prediction of the wind farm power output in various wind conditions is needed in the layout design phase, which in practice is realized by computationally cheap analytical methods. Specifically, the wake velocity deficits caused by the individual wind turbines are first computed from analytical wake models, and then superimposed to get the total wake deficit (Jensen 1983; Niayifar & Porté-Agel 2016), as sketched in figure 1.

† Email address for correspondence: haohua_zong@126.com

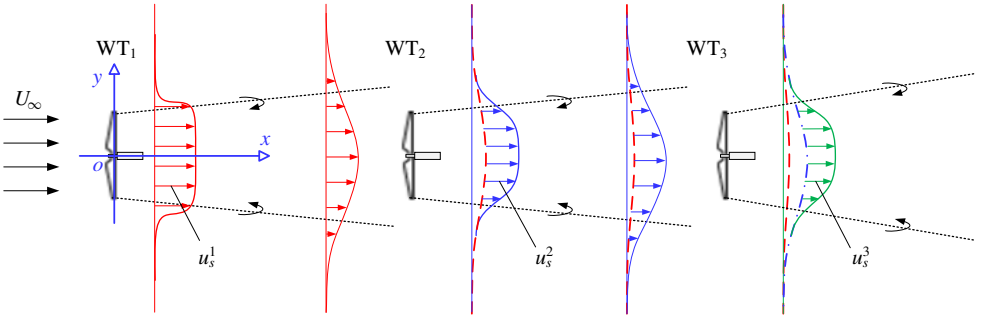

FIGURE 1. Sketch of wake superposition in a three-row wind farm. Here, u_s^i denotes the wake velocity deficit caused by the ith wind turbine.

Depending on the reference wind speed used to calculate the individual wakes (either local or global) and the operations adopted to combine the wakes (either summing the wake velocity deficits, or summing the squares of the wake velocity deficits), four wake superposition methods are available in the literature (Stevens & Meneveau 2017; Porté-Agel *et al.* 2019), as follows.

$$\text{Method A: } U_w(x,y,z) = U_\infty - \sum_i (U_\infty - u_w^i(x,y,z)). \tag{1.1}$$

$$\text{Method B: } U_w(x,y,z) = U_\infty - \sqrt{\sum_i (U_\infty - u_w^i(x,y,z))^2}. \tag{1.2}$$

$$\text{Method C: } U_w(x,y,z) = U_\infty - \sum_i (u_0^i - u_w^i(x,y,z)). \tag{1.3}$$

$$\text{Method D: } U_w(x,y,z) = U_\infty - \sqrt{\sum_i (u_0^i - u_w^i(x,y,z))^2}. \tag{1.4}$$

Here, u_0^i is the mean wind velocity perceived by the ith wind turbine (referred to as WT_i hereinafter); u_w^i is the wake velocity induced by WT_i in stand-alone conditions. The difference between the incoming wind velocity and the wake velocity defines the individual wake velocity deficit, i.e. $u_s^i = u_0^i - u_w^i$.

The logic behind each of these methods is briefly explained here. In Method A (Lissaman 1979), a large wind turbine spacing with weak wake interaction is assumed, such that, during the calculation of individual wakes, the mean wind velocity experienced by the downstream wind turbines can be substituted by the inflow velocity of the wind farm, i.e. $u_0^i \approx U_\infty$. Further, since the wake velocity deficit is small, the momentum deficit term $(U_\infty - u_s^i) \cdot u_s^i$ can be approximated by $U_\infty \cdot u_s^i$. Consequently, to conserve the total momentum deficit in the wake (i.e. total wind turbine thrust), one only needs to sum the wake velocity deficits linearly, like a passive scalar. Method B (Katic, Højstrup & Jensen 1987) makes a similar assumption of $u_0^i \approx U_\infty$ during the calculation of individual wakes. Nevertheless, the wake superposition is realized by summing the squares of the wake velocity deficits. By executing this operation, the authors expected to conserve the mean kinetic energy deficit during wake interaction, which is disputable as the mean kinetic energy flux is not conserved in wake flows due to the non-trivial turbulent dissipation.

The counterparts of Methods A and B are Methods C and D proposed by Niayifar & Porté-Agel (2016) and Voutsinas, Rados & Zervos (1990), respectively. In these two recent methods, similar operations (i.e. linear sum and square sum) are adopted to combine the individual wake velocity deficits without theoretical justification. Nevertheless, during the computation of the individual wakes, the approximation of $u_0^i \approx U_\infty$ is removed, and the mean wind speeds perceived by the wind turbines u_0^i ($i = 0, 1, 2, \ldots$) are determined consecutively from upstream to downstream. Therefore, it is largely expected that Methods C and D will give more accurate predictions of the wind farm power production than their counterparts, particularly in the cases of short wind turbine spacing and large wake velocity deficit.

To summarize, the four existing wake superposition methods are all empirical relations without solid theoretical foundation. During the combination of individual wakes, the total momentum deficit is highly unlikely to be conserved by these methods, which could introduce significant errors in the power prediction of wind farms. In this study, a novel wake superposition method is derived rigorously from the law of conservation of momentum and its superior performance over the other four existing methods is demonstrated by experimental and large-eddy simulation (LES) data.

2. Theoretical derivation

2.1. *Linearized expression for the momentum deficit flux*

For wake flow, the law of conservation of momentum stipulates that the total momentum deficit flux across the wake cross-section has to be a conserved quantity, equalling the drag imposed to the flow (Pope 2000). Applying this principle to each of the wind turbines shown in figure 1, equation (2.1) can be derived (for details, please refer to appendix A),

$$T_i = \rho \iint u_w^i(x, y, z) \cdot u_s^i(x, y, z)\, \mathrm{d}y\, \mathrm{d}z, \tag{2.1}$$

where T_i denotes the thrust of WT_i. Since the wake velocity u_w is correlated with the wake velocity deficit, the relationship between T_i and u_s^i is nonlinear. However, if an appropriate mean wake convection velocity (denoted as u_c^i) is selected to represent the spatially dependent wake velocity in the entire wake cross-section, equation (2.1) may be rewritten in the following linear form:

$$T_i = \rho \iint u_c^i(x) \cdot u_s^i(x, y, z)\, \mathrm{d}y\, \mathrm{d}z = \rho u_c^i(x) \iint u_s^i(x, y, z)\, \mathrm{d}y\, \mathrm{d}z. \tag{2.2}$$

Substituting (2.2) into (2.1), a mathematical definition of the mean wake convection velocity is given as follows:

$$u_c^i(x) = \frac{\iint u_w^i(x, y, z) \cdot u_s^i(x, y, z)\, \mathrm{d}y\, \mathrm{d}z}{\iint u_s^i(x, y, z)\, \mathrm{d}y\, \mathrm{d}z}. \tag{2.3}$$

Namely, the mean convection velocity necessary for linearizing the momentum deficit term is a weighted average of the wake velocity, where the weights are selected as the corresponding wake velocity deficits. Since the analytical expressions

for u_w^i and u_s^i are widely available in various wind turbine wake models (Jensen 1983; Frandsen *et al.* 2006; Bastankhah & Porté-Agel 2014), the expression for u_c^i can also be derived in different forms. Nevertheless, for the purpose of accurate wind farm power prediction, only the wake models that are derived strictly from the law of conservation of momentum (i.e. excluding the Jensen model) are recommended. Here, the Gaussian wake model proposed by Bastankhah & Porté-Agel (2014) is taken as an example. The wake velocity deficit behind the ith wind turbine reads as

$$\frac{u_s^i}{u_0^i} = \left(1 - \sqrt{1 - \frac{C_t^i}{8\sigma_y\sigma_z/D^2}}\right) \cdot \exp\left(-\frac{y^2}{2\sigma_y^2} - \frac{z^2}{2\sigma_z^2}\right), \tag{2.4}$$

where D is the rotor diameter; C_t^i is the thrust coefficient WT_i; σ_y and σ_z denote the wake width in the spanwise and vertical directions, respectively. Substituting (2.4) into (2.3), an explicit expression for the mean convection velocity can be obtained:

$$\frac{u_c^i(x)}{u_0^i} = \frac{1}{2} + \frac{1}{2}\sqrt{1 - \frac{C_t^i}{8\sigma_y\sigma_z/D^2}}. \tag{2.5}$$

As a result, the mean wake convection velocity is bounded between $0.5u_0^i$ and u_0^i, increasing with the wake width and decreasing with the thrust coefficient.

2.2. *Momentum-conserving wake superposition principle*

To conserve the total momentum deficit (i.e. wind turbine thrust) during wake superposition, the combined wake velocity U_w has to satisfy the following equation:

$$\rho \iint U_w(x, y, z) \cdot U_s(x, y, z)\,\mathrm{d}y\,\mathrm{d}z = \sum_i T_i = \sum_i \rho u_c^i(x) \iint u_s^i(x, y, z)\,\mathrm{d}y\,\mathrm{d}z, \tag{2.6}$$

where U_s is the total wake velocity deficit given by $U_\infty - U_w$. Analogous to (2.3), a mean convection velocity for the combined wake (U_c) can be defined as follows:

$$U_c(x) = \frac{\iint U_w(x, y, z) \cdot U_s(x, y, z)\,\mathrm{d}y\,\mathrm{d}z}{\iint U_s(x, y, z)\,\mathrm{d}y\,\mathrm{d}z}. \tag{2.7}$$

Using this relation to simplify (2.6), the following equation is derived:

$$\iint U_s(x, y, z)\,\mathrm{d}y\,\mathrm{d}z = \sum_i \frac{u_c^i(x)}{U_c(x)} \iint u_s^i(x, y, z)\,\mathrm{d}y\,\mathrm{d}z. \tag{2.8}$$

At this stage, it becomes evident that, in order to conserve the total momentum during wake superposition, the following expression should be used:

$$U_s(x, y, z) = \sum_i \frac{u_c^i(x)}{U_c(x)} u_s^i(x, y, z). \tag{2.9}$$

Equation (2.9) states that the total wake velocity deficit equals a weighted sum of the individual wake velocity deficits, where the weights are determined by the ratio of u_c^i to U_c. This is understandable since, when combining two wakes with the same amount of velocity deficit, the one with the larger convection velocity carries more momentum deficit, and thus should be represented by a higher weight during the velocity deficit addition. In the case of small wake velocity deficits (say, $u_s^i \leqslant 0.1U_\infty$), u_c^i/U_c may be approximated by 1, and the above expression automatically becomes (1.3) (Method C). However, this only happens when the wind turbine spacing exceeds $15D$ (Chamorro & Porté-Agel 2010). Additionally, since the mean convection velocity for the combined wake is unknown prior to wake superposition, an iterative method should be deployed to solve the combined wake velocity out of (2.7) and (2.9). Specifically, U_c is initialized to be the maximum value of u_c^i and substituted into (2.9) to get an estimated total wake velocity deficit. The estimated total wake velocity deficit is further plugged into (2.7) to get a corrected convection velocity for the combined wake U_c^*. This iterative correction repeats, until a certain criterion is met (e.g. $|U_c - U_c^*|/U_c^* \leqslant 0.001$). Typically, no more than five iterations are needed to reach convergence, and the corresponding computation cost is negligible compared to the individual wake computation.

3. Model validation

3.1. *Particle imaging velocimetry measurements in a three-row wind farm*

For validation purposes, the three-row wind farm sketched in figure 1 is constructed in the boundary layer wind tunnel at the WIRE laboratory of EPFL, using the miniature wind turbines designed by Bastankhah & Porté-Agel (2017) (WIRE-01, rotor diameter: 0.15 m, hub height: 0.125 m), and the velocity field at the hub-height is measured by a particle imaging velocimetry (PIV) system. The time-averaged wind speed and the turbulence intensity at the hub level are kept at 4.9 m s^{-1} and 6 %, respectively. The boundary layer thickness, determined by 99 % of the free-stream velocity, is approximately 0.3 m. The streamwise spacing between the wind turbines is fixed at $5D$, and the optimal rotation speed of each wind turbine is set *in situ* based on the free rotation speed, following the procedure described in Bastankhah & Porté-Agel (2019). The thrust and power coefficients (denoted as C_t and C_p) of the WIRE-01 turbine at optimal operation are 0.82 and 0.35, respectively (Bastankhah & Porté-Agel 2016). The PIV system consists of a camera (LaVision-sCMOS), a Litron laser (Nano TRL 425-10) and a programmable timing unit (PTU-v9, LaVision). Both the camera and the laser are mounted on a traversing system, to shift the field of view (FOV) in the streamwise direction. In total, three sets of FOVs are arranged to cover the complete wake evolution in an area of $15D \times 5D$. In each FOV, 500 image pairs are recorded to get statistically converged mean velocity fields.

The aforementioned model wind farm is used as a test bench to examine the performance of different wake superposition methods. The individual wake velocity deficits are computed from (2.4) (Bastankhah & Porté-Agel 2014), and the wake width is modelled as a quasi-linear function of the streamwise coordinate (Shapiro, Gayme & Meneveau 2018):

$$\left.\begin{aligned} \frac{\sigma_y}{D} &= 0.35\cos\beta + k_w \ln\left[1+\exp\left(\frac{x-x_{th}}{D}\right)\right], \\ \frac{\sigma_z}{D} &= 0.35 + k_w \ln\left[1+\exp\left(\frac{x-x_{th}}{D}\right)\right], \end{aligned}\right\} \tag{3.1}$$

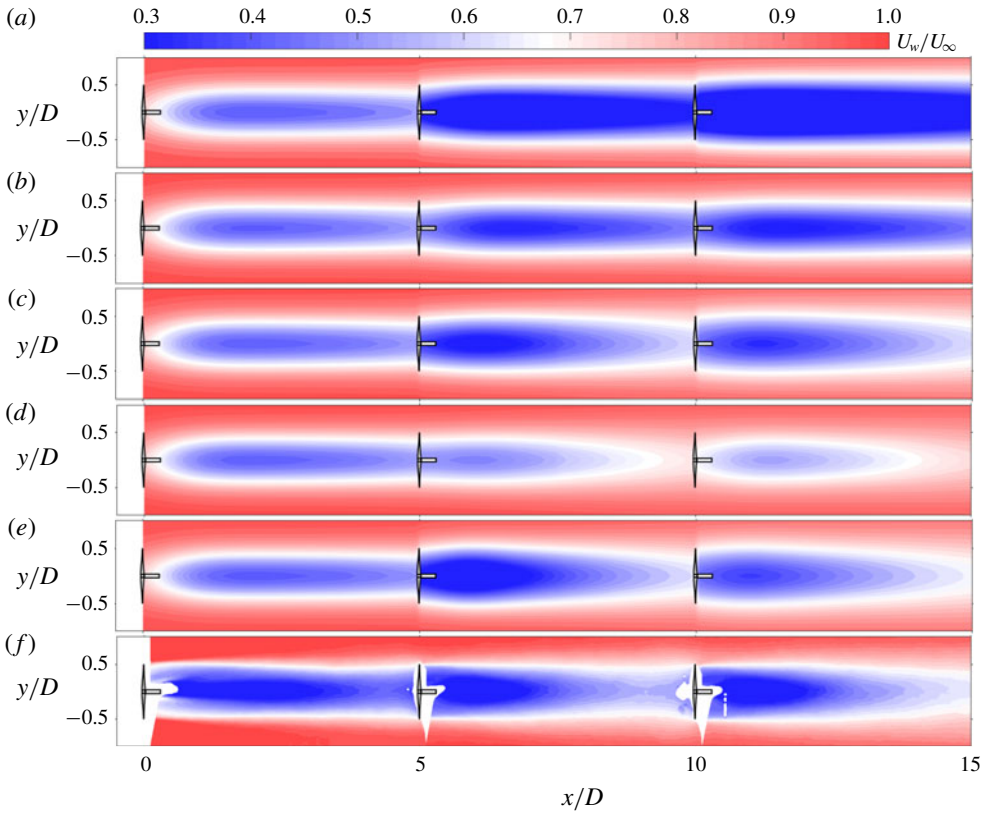

FIGURE 2. Middle-hub wake velocity contours obtained from: (*a*) Method A (Lissaman 1979), (*b*) Method B (Katic *et al.* 1987), (*c*) Method C (Niayifar & Porté-Agel 2016), (*d*) Method D (Voutsinas *et al.* 1990), (*e*) the proposed new method, and (*f*) particle imaging velocimetry measurements.

where β, k_w and x_{th} denote the yaw angle, the wake spreading rate and the near-wake length, respectively.

Namely, in the near wake, the wake width remains approximately constant, whereas in the far wake, the wake width grows linearly with an asymptotic wake spreading rate of k_w. The detailed expression for x_{th} is available in Vermeulen (1980). The wake spreading rate is associated with both the ambient turbulence intensity I_0 and the added turbulence intensity I_+, and can be modelled as $k_w = 0.38(I_0^2 + I_+^2)^{1/2} + 0.004$, where $I_+ = 0.73a^{0.83}I_0^{0.03}(x/D)^{-0.32}$ (Niayifar & Porté-Agel 2016). Additionally, to simulate the effect of the near-wake pressure gradient, the thrust coefficients in (2.4)–(2.5) are written as an error function of the streamwise coordinate, $C_t^i(x) = 0.82(1 + \mathrm{erf}(x/D))/2$, to create a gradual increase of the wake deficit at $x < 2D$ (Shapiro *et al.* 2018).

Figure 2 shows the middle-hub velocity fields computed with analytical methods and measured by PIV. As a result of the low ambient turbulence intensity, the near-wake region of WT_1 extends to more than $3D$ (figure 2*f*). In the centreline of this near-wake region, a rather low wake velocity is noticed, which is related to the hub drag. The performance of different wake superposition methods can be

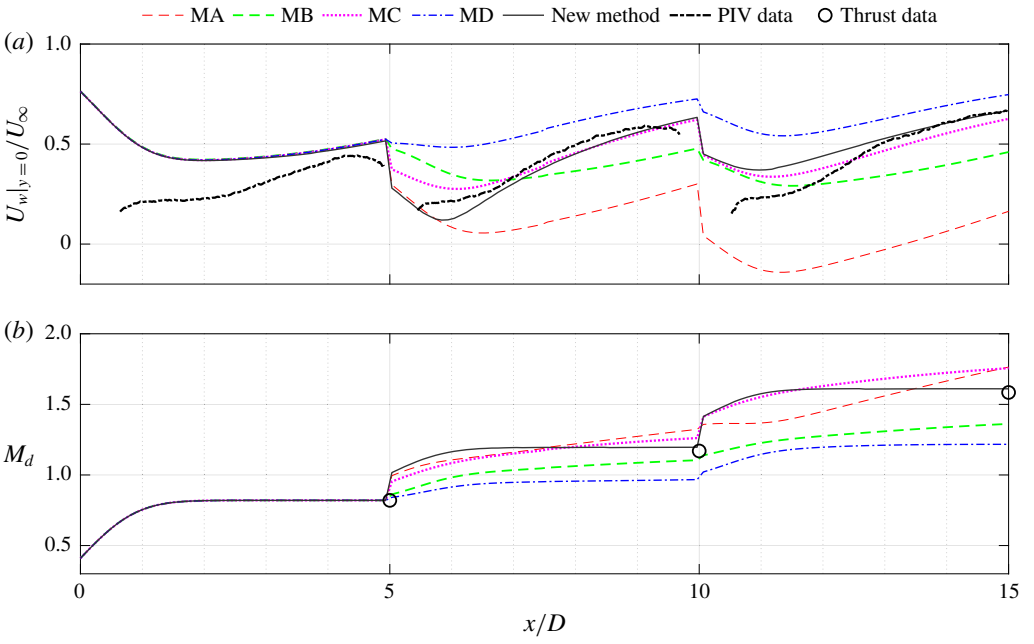

FIGURE 3. Streamwise variations of (*a*) the centreline wake deficit, (*b*) the normalized total momentum deficit. Methods A–D are abbreviated as MA–MD in the legends.

appreciated by comparing the wake velocity contours behind WT_2 and WT_3, where, due to the increase of turbulence intensity, a short near wake and a fast wake recovery are expected. Methods A and B from Lissaman (1979) and Katic *et al.* (1987) fail to reproduce these two phenomena, since the interactions between wind turbines are neglected during the calculation of individual wakes. Method D (Voutsinas *et al.* 1990) delivers a reasonable trend of the near-wake length, whereas the wake velocity deficit is largely underestimated, compared to the experimental data. Consequently, Method C (Niayifar & Porté-Agel 2016) and the proposed new method are the only two methods capable of delivering a satisfactory wind farm wake flow.

Quantitative comparison of the centreline wake velocity (i.e. $U_w|_{y=0}$) is made in figure 3(*a*). As shown, the centreline wake velocity deficit is largely overestimated by Methods A and B, since both of them fail to account for the fact that the local wind speeds perceived by the downstream wind turbines are always lower than the inflow velocity. Method D, on the contrary, underestimates the centreline wake velocity deficit, which is consistent with the observation in Niayifar & Porté-Agel (2016). Method C and the proposed new method outperform the other methods by delivering a satisfactory prediction of the centreline wake velocity deficit in the range $7 \leqslant x/D \leqslant 10$. Nevertheless, the difference in their performance starts to stand out at $x/D \leqslant 13$, where the wake velocity predicted by Method C is always 5 % lower than that obtained from the experiment and the new method. This 5 % discrepancy, although still acceptable in the current context, can accumulate to large errors when more turbine rows are added, as will be demonstrated in § 3.2.

Based on the models results shown in figure 2, the normalized total momentum deficit ($\overline{M}_d$) is computed by the following equation:

$$\overline{M}_d = \frac{8 \iint U_w \cdot (U_\infty - U_w)\,\mathrm{d}y\,\mathrm{d}z}{U_\infty^2 \pi D^2}, \tag{3.2}$$

where the initial momentum flux across the rotor disk is selected for normalization, analogous to the definition of the wind turbine thrust coefficient.

Theoretically, the total momentum deficit should exhibit a stair-step increase along the streamwise direction, with each step corresponding to the additional thrust/drag induced by a new turbine row. Therefore, to validate the model predictions of $\overline{M}_d$, experimental values of the turbine thrust are required. In the present study, force measurements are not performed, and the power measurement data available in Bastankhah & Porté-Agel (2019) are used to estimate the turbine thrust. Specifically, based on the definitions of C_t and C_p (0.82 and 0.35 respectively for the WIRE-01 turbine at optimal operation), we have the following two equations:

$$\left.\begin{aligned} P_i &= C_p \cdot \frac{\rho (u_0^i)^3}{2} \cdot \frac{\pi D^2}{4}, \\ T_i &= C_t \cdot \frac{\rho (u_0^i)^2}{2} \cdot \frac{\pi D^2}{4}, \end{aligned}\right\} \tag{3.3}$$

where P_i denotes the power production of the ith turbine ($i = 1, 2, 3$). Working out the mean wind speed from the first equation and substituting into the second one, the relation between T_i and P_i can be derived:

$$T_i = C_t \cdot \left(\frac{\rho \pi D^2}{8}\right)^{1/3} \cdot \left(\frac{P_i}{C_p}\right)^{2/3}. \tag{3.4}$$

Figure 3 compares the normalized total momentum deficits computed with the analytical models and derived directly from the turbine thrust. Of all the five wake superposition methods, only the one proposed in this study is able to collapse with the thrust data and conserve the total momentum deficit during wake superposition. For Methods B and D, the total wake deficit is decreased after the superposition, whereas for Method A, the total momentum deficit keeps increasing unrealistically. Method C, which serves as a simplified form of the proposed new method in cases of large wind turbine spacing (more than $15D$), also exhibits a slightly increasing trend of the total momentum deficit, which directly leads to the wake velocity deficit overestimation at $x/D \leqslant 13$ (see figure 3*a*).

3.2. *LES results for the Horns-Rev wind farm*

In this section, the LES results for a large wind farm, Horns-Rev (Porté-Agel, Wu & Chen 2013), are used as a benchmark to evaluate the performance of different wake superposition methods. The Horns-Rev wind farm has a rhomboid layout, consisting of 80 wind turbines arranged in 10 rows and 8 columns. Along both the row and column directions, the spacing between two adjacent turbines is seven rotor diameters (Barthelmie *et al.* 2010). To compute the power production of this wind farm, the major parameters are inherited from Porté-Agel *et al.* (2013), including the ambient

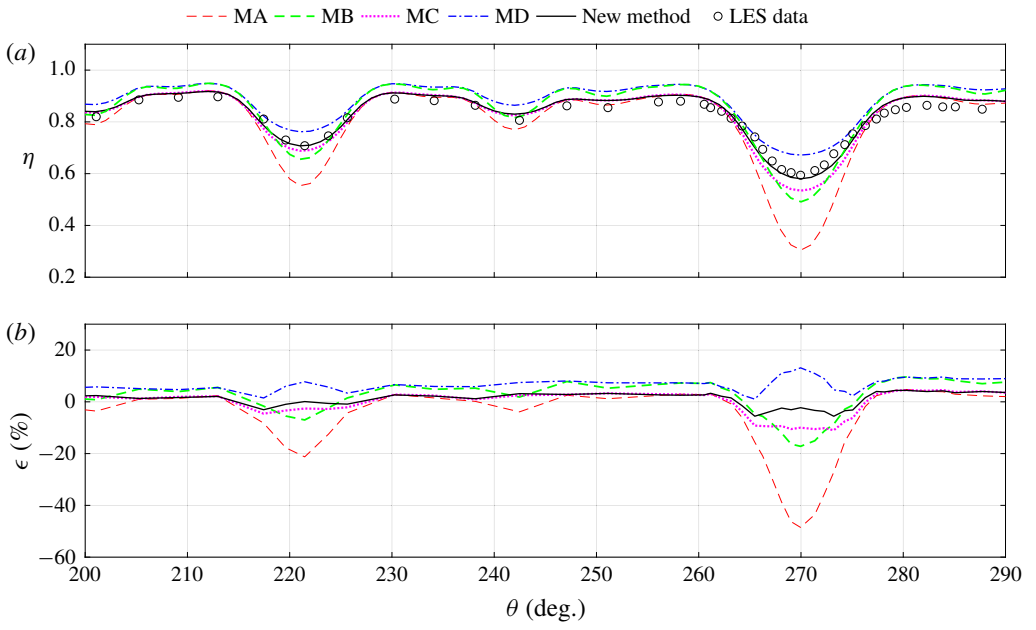

FIGURE 4. (*a*) Comparison of the Horns-Rev wind farm efficiency (η) predicted by different wake superposition methods. Here, θ denotes the wind direction, with 270° corresponding to western winds. (*b*) Relative error between the model predictions and the LES data at different wind directions.

turbulence intensity (7.7 %), mean hub-height velocity (8 m s^{-1}) and turbine thrust coefficient (0.8). Other parameters, e.g. the initial wake width, remain the same as those used in § 3.1.

The wind farm efficiencies (denoted as η) predicted by the LES and analytical wind farm model using different wake superposition methods are shown in figure 4(*a*). Significant power losses are noticed in the vicinity of 222° and 270°, which involve full-wake interactions in a streamwise distance of less than 10*D*. Within these two wind sectors, the wind farm efficiency predicted by the new method collapses remarkably well with the LES data, whereas for the other methods, a noticeable discrepancy still exists. To quantitatively examine these discrepancies, the relative power prediction error (denoted as ϵ, in units of percentage) is plotted in figure 4(*b*). Consistent with the wake velocity deficit analysis in § 3.1, Methods A, B and C exhibit an overestimation of the wake-induced power losses, whereas Method D gives an underestimation. As the streamwise spacing between two interacting wind turbines decreases (270° versus 222°), the relative power prediction error increases.

Figure 5 shows the normalized power production of each turbine row (denoted as $\overline{P}_i$), at a representative wind direction of $\theta = 270°$. As indicated by the LES results, the power production first drops and then remains approximately unchanged. The proposed new method, once again, outperforms the other methods by closely following the trend stipulated by LES. For Methods A and C, since the individual wake velocity deficits are directly summed, the total wake velocity deficit keeps accumulating unrealistically in the streamwise direction, leading to a decreasing trend of the power production. As a comparison, for Methods B and D, due to the usage of a square-sum operation in the combination of individual wake velocity deficits,

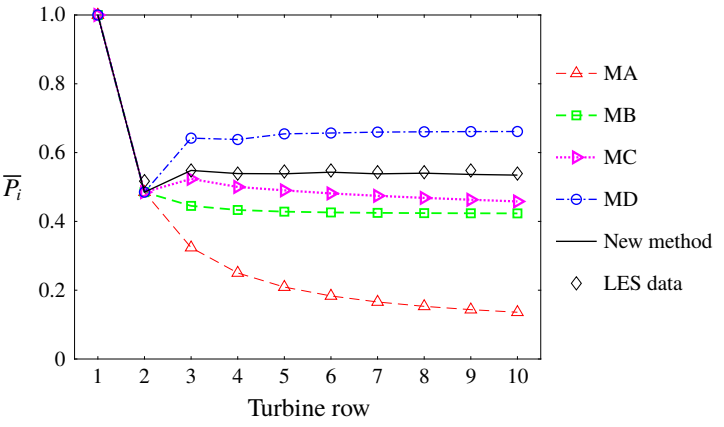

FIGURE 5. Normalized power production for different turbine rows.

the predicted power production quickly reaches a plateau after three turbine rows. Nevertheless, this plateau value deviates noticeably from that in the LES results.

4. Extension to wake deflection superposition

Active wake control has been increasingly recognized as an effective technique to mitigate the unfavourable wake interactions in wind farms. Bay *et al.* (2019) demonstrated that, to accurately predict the power production subject to active wake control, it is crucial to include the 'secondary steering effect' sketched in figure 6(*a*), where, as the upstream wind turbine WT_1 yaws, the wake trajectory of a non-yawed downstream wind turbine WT_2 deviates from its rotor centreline. This unexpected wake deflection, originating from the non-vanishing transverse velocity induced by WT_1 at the position of WT_2, underlies the necessity of wake deflection superposition. Starting from the simplified spanwise momentum equation derived in appendix (A 4) and following a similar procedure as described in § 2, the superposition principle of v^i can be derived, as follows:

$$V(x, y, z) = \sum_i \frac{u_c^i(x)}{U_c(x)} v^i(x, y, z), \tag{4.1}$$

where V is the spatially dependent transverse velocity for the combined wake. This equation, together with (2.9), reiterates that a weighed sum should be used to combine the individual transverse velocity/wake velocity deficits, instead of a direct sum.

In the current wake models of yawed wind turbines, the wake deflection is typically integrated from the slope of the wake trajectory, defined as the ratio of the wake-centre transverse velocity to the mean convection velocity, as sketched in figure 6(*a*). Following this route and applying (4.1) to the wake centre of the jth wind turbine (x_c^j, y_c^j), the total transverse velocity experienced by the wake of WT_j (V_c^j) can be obtained:

$$V_c^j(x_c^j, y_c^j) = \sum_i \frac{u_c^i(x_c^j)}{U_c(x_c^j)} v^i(x_c^j, y_c^j). \tag{4.2}$$

It is evident from (4.2) that, in order to derive the total wake deflection, the mean convection velocity for the combined wake (U_c) has to be known *a priori*, which

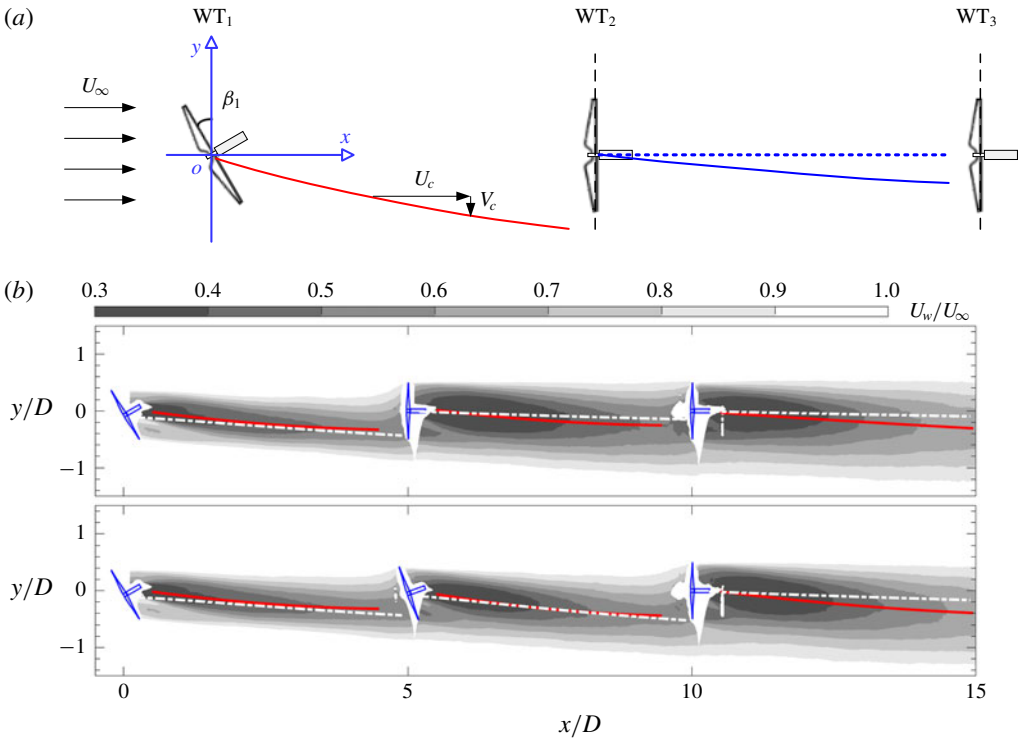

FIGURE 6. (*a*) Sketch of the secondary steering effect. The wake trajectories of WT_1 and WT_2 are indicated by the solid lines. (*b*) Wake velocity fields measured at the hub level. Top plot (Case 1): $\beta_1 = 30°$, $\beta_2 = 0°$, $\beta_2 = 0°$. Bottom plot (Case 2): $\beta_1 = 30°$, $\beta_2 = 20°$, $\beta_2 = 0°$. The red solid lines and the white dash-dot lines represent the wake trajectories extracted from PIV data and computed by (4.3), respectively.

is impossible as U_c is dependent on the spatial distributions of the individual wake velocity deficits and thus can only be computed once the wake deflection is given. In principle, an iterative method should be deployed to reconcile this conflict. However, to avoid increasing the computational cost, u_c^i/U_c is approximated by u_0^i/u_0^j, and the slope of the wake trajectory of WT_j is written as

$$\frac{\mathrm{d}y_c^j}{\mathrm{d}x_c^j} \approx \frac{V_c^j}{u_0^j} \approx \sum_i \frac{u_0^i}{u_0^j u_0^j} v^i(x_c^j, y_c^j). \tag{4.3}$$

Currently, several models are available to compute the transverse velocity induced by a stand-alone yawed wind turbine (i.e. v^i) (Jiménez, Crespo & Migoya 2010; Bastankhah & Porté-Agel 2016; Shapiro *et al.* 2018). For the sake of simplicity, the following expression adapted from Shapiro *et al.* (2018) is used in this investigation:

$$v^i(x, y) = \frac{-C_t^i u_0^i \cos^2\beta_i \sin\beta_i}{8\sigma_y\sigma_z/\sigma_{y0}\sigma_{z0}} \cdot \left[1 + \mathrm{erf}\left(\frac{x}{D}\right)\right] \cdot \exp\left(-\frac{(y - y_c^i)^2}{2\sigma_y^2}\right), \tag{4.4}$$

where σ_{y0} and σ_{z0} are the initial wake widths along the spanwise and vertical directions, respectively. Different from the original expression, a Gaussian function

(i.e. $\exp(-(y-y_c^i)^2/2\sigma_y^2)$) is added here, to spread the transverse velocity in the spanwise direction and thus generalize the wake deflection superposition to partial wake conditions.

The three-row model wind farm described in § 3.1 is used once again as a test bench to validate the proposed method of wake deflection superposition. Two cases are selected to execute PIV measurements. In the first case, only the most upstream wind turbine is yawed at $\beta_1 = 30°$. In the second case, both WT_1 and WT_2 are actuated, and the optimal yaw angle list for the maximum power production ($\beta_1 = 30°$, $\beta_2 = 20°$, $\beta_3 = 0°$) reported in Bastankhah & Porté-Agel (2019) is adopted. Figure 6(*b*) compares the wake trajectories extracted from the PIV measurements and obtained by (4.3). In both cases, the secondary steering effect is successfully reproduced by the proposed analytical method, and the wake deflections of the first two wind turbines (y_c) are predicted within a mean error of less than $0.05D$. For the last wind turbine, the measured wake deflection is higher than the model prediction, which can be attributed to the spanwise wind shear. Specifically, when the wake of WT_2 shifts preferably to the negative y-direction, the lower half of WT_3 perceives a lower wind speed than the upper half. Due to this noticeable wind shear, different levels of turbulent kinetic energy are generated on the two sides of the wake of WT_3, leading to uneven wake recovery rates. As a result, larger/smaller wake velocity deficits are exhibited on the side with a lower/higher wake recovery rate, resulting in an additional shift of the wake centre, independent from that caused by the non-vanishing transverse velocity induced by the upstream yawed wind turbines.

5. Summary

In this study, a novel wake superposition method is derived rigorously from the law of conservation of momentum. The total wake velocity deficit is expressed as a weighted sum of the individual wake velocity deficits, where the weight equals to the ratio of the characteristic convection velocity of the individual wake to that of the combined wake. The performance of this new method is validated against the PIV data obtained in a three-row model wind farm and the LES results pertaining to the Horns-Rev wind farm. Detailed comparisons show that, except for the near-wake region where the pressure gradient is non-trivial, the proposed wake superposition method can give a rather accurate prediction of the centreline wake velocity deficit. The maximum power prediction error in the case of the Horns-Rev wind farm is reduced to as low as 5 %. None of the wake superposition methods available in the literature is able to achieve such a high accuracy, largely because of their inability to conserve the total momentum deficit during wake superposition. Additionally, the momentum-conserving wake superposition principle has been extended to combine the transverse velocities induced by yawed wind turbines, and the secondary wake steering effect crucial to active wake control is successfully reproduced.

Acknowledgements

This research was funded by the Swiss National Science Foundation (grant number: 200021_172538) and the Swiss Federal Office of Energy. In addition, this project was carried out within the frame of the Swiss Centre for Competence in Energy Research on the Future Swiss Electrical Infrastructure (SCCER-FURIES) with the financial support of the Swiss Innovation Agency (Innosuisse – SCCER programme, contract number: 1155002544).

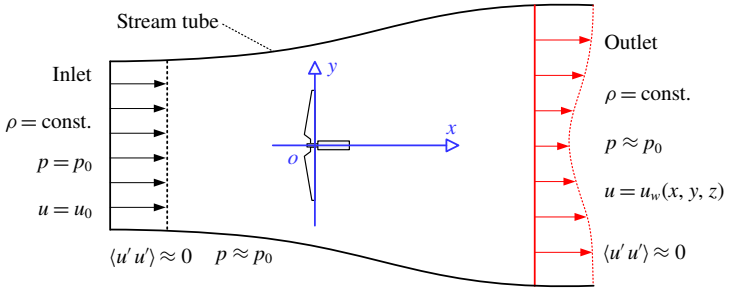

FIGURE 7. The control volume and boundary conditions used to derive the simplified momentum equations for wake flow.

Declaration of interests

The authors report no conflict of interest.

Appendix A. Simplified momentum equations for wake flow

A sufficiently large stream tube enclosing the entire wind turbine is selected as the control volume, as sketched in figure 7. Only uniform inflow is considered, which is one of the inherent assumptions made to derive the analytical wind turbine wake models (Jensen 1983; Frandsen *et al.* 2006; Bastankhah & Porté-Agel 2014). The inlet of the stream tube is placed far away from the induction zone of the turbine, such that both the static pressure and the inlet velocity remain unaffected and can be treated as ambient values of $p = p_0$ and $u = u_0$. Similarly, the outlet is positioned in the far wake, where the static pressure deviates marginally from the ambient pressure, i.e. $p \approx p_0$. The turbulent momentum transportation contributed by the Reynolds normal stress term $\langle u'u' \rangle$ is typically small compared to the mean momentum transportation ($O(u_0^2)$), and, thus, can be readily neglected (Tennekes & Lumley 1972). In addition, since the stream tube is selected to be sufficiently large, the pressure disturbances and turbulent shear stresses generated by wakes will not be felt by the side boundaries, leading to zero pressure force and zero turbulent momentum transfer in the spanwise and vertical directions, i.e. $\langle u'v' \rangle \approx 0$ and $\langle u'w' \rangle \approx 0$.

Based on the above assumptions, the integral form of the streamwise momentum equation (Anderson 2010), when applied to the control volume shown in figure 7, can be simplified as follows:

$$\rho \iint_{inlet} u_0^2 \, \mathrm{d}y \, \mathrm{d}z - \rho \iint_{outlet} u_w(x, y, z)^2 \, \mathrm{d}y \, \mathrm{d}z = T, \tag{A 1}$$

where T denotes the turbine thrust in the streamwise direction. Essentially, equation (A 1) states that the total momentum difference between the inlet and outlet of the stream tube equals the drag imposed to the flow. Further, applying the law of conservation of mass to the control volume, we have

$$\rho \iint_{inlet} u_0 \, \mathrm{d}y \, \mathrm{d}z = \rho \iint_{outlet} u_w(x, y, z) \, \mathrm{d}y \, \mathrm{d}z. \tag{A 2}$$

Substituting (A 2) into (A 1), the following expression can be obtained:

$$T = \rho \iint_{outlet} u_w(x, y, z) \cdot u_s(x, y, z) \, \mathrm{d}y \, \mathrm{d}z. \tag{A 3}$$

In the case of a yawed wind turbine, a similar expression for the lateral turbine thrust (denoted as F) can be derived from the spanwise momentum equation. In particular, there is no spanwise momentum flowing into the control volume, and the total spanwise momentum integrated over the outlet is directly balanced out by the lateral force F, which reads as

$$F = \rho \iint_{outlet} u_w(x, y, z) \cdot v(x, y, z)\, \mathrm{d}y\, \mathrm{d}z. \tag{A 4}$$

REFERENCES

ANDERSON, J. D. 2010 *Fundamentals of Aerodynamics*. Tata McGraw-Hill Education.

BARTHELMIE, R. J., PRYOR, S. C., FRANDSEN, S. T., HANSEN, K. S., SCHEPERS, J. G., RADOS, K., SCHLEZ, W., NEUBERT, A., JENSEN, L. E. & NECKELMANN, S. 2010 Quantifying the impact of wind turbine wakes on power output at offshore wind farms. *J. Atmos. Ocean. Technol.* **27** (8), 1302–1317.

BASTANKHAH, M. & PORTÉ-AGEL, F. 2014 A new analytical model for wind-turbine wakes. *J. Renew. Energy* **70**, 116–123.

BASTANKHAH, M. & PORTÉ-AGEL, F. 2016 Experimental and theoretical study of wind turbine wakes in yawed conditions. *J. Fluid Mech.* **806**, 506–541.

BASTANKHAH, M. & PORTÉ-AGEL, F. 2017 A new miniature wind turbine for wind tunnel experiments. Part I: Design and performance. *Energies* **10** (7), 908.

BASTANKHAH, M. & PORTÉ-AGEL, F. 2019 Wind farm power optimization via yaw angle control: a wind tunnel study. *J. Renew. Sustain. Energy* **11** (2), 023301.

BAY, C., KING, J., FLEMING, P., MUDAFORT, R. & MARTINEZ, L. 2019 Unlocking the full potential of wake steering: implementation and assessment of a controls-oriented model. *Tech. Rep.* NREL/JA-5000-73777. National Renewable Energy Lab, USA.

CHAMORRO, L. P. & PORTÉ-AGEL, F. 2010 Effects of thermal stability and incoming boundary-layer flow characteristics on wind-turbine wakes: a wind-tunnel study. *Boundary-Layer Meteorol.* **136** (3), 515–533.

FRANDSEN, S., BARTHELMIE, R., PRYOR, S., RATHMANN, O., LARSEN, S., HØJSTRUP, J. & THØGERSEN, M. 2006 Analytical modelling of wind speed deficit in large offshore wind farms. *Wind Energy* **9** (1–2), 39–53.

JENSEN, N. O. 1983 A note on wind turbine interaction. *Tech. Rep.* Ris-M-2411. Risoe National Laboratory.

JIMÉNEZ, Á., CRESPO, A. & MIGOYA, E. 2010 Application of a LES technique to characterize the wake deflection of a wind turbine in yaw. *Wind Energy* **13** (6), 559–572.

KATIC, I., HØJSTRUP, J. & JENSEN, N. O. 1987 A simple model for cluster efficiency. In *European Wind Energy Association Conference and Exhibition*. A. Raguzzi.

LISSAMAN, P. B. S. 1979 Energy effectiveness of arbitrary arrays of wind turbines. *J. Energy* **3** (6), 323–328.

NIAYIFAR, A. & PORTÉ-AGEL, F. 2016 Analytical modeling of wind farms: a new approach for power prediction. *Energies* **9** (9), 741.

POPE, S. B. 2000 *Turbulent Flows*. Cambridge University Press.

PORTÉ-AGEL, F., BASTANKHAH, M. & SHAMSODDIN, S. 2019 Wind-turbine and wind-farm flows: a review. *Boundary-Layer Meteorol.* **174** (1), 1–59.

PORTÉ-AGEL, F., WU, Y.-T. & CHEN, C.-H. 2013 A numerical study of the effects of wind direction on turbine wakes and power losses in a large wind farm. *Energies* **6** (10), 5297–5313.

SHAPIRO, C. R., GAYME, D. F. & MENEVEAU, C. 2018 Modelling yawed wind turbine wakes: a lifting line approach. *J. Fluid Mech.* **841**, R1.

STEVENS, R. J. & MENEVEAU, C. 2017 Flow structure and turbulence in wind farms. *Annu. Rev Fluid Mech.* **49**, 311–339.

TENNEKES, H. & LUMLEY, J. L. 1972 *A First Course in Turbulence*. MIT Press.

VERMEULEN, P. E. J. 1980 An experimental analysis of wind turbine wakes. In *3rd International Symposium on Wind Energy Systems, Lyngby, Denmark*, pp. 431–450.

VOUTSINAS, S., RADOS, K. & ZERVOS, A. 1990 On the analysis of wake effects in wind parks. *Wind Engng* 204–219.